Mechanics Research Communications 80 (2017) 38–46

Contents lists available at ScienceDirect

Mechanics Research Communications

journal homepage: www.elsevier.com/locate/mechrescom

A phase-field modeling approach of hydraulic fracture in saturated porous media

Y. Heider*, B. Markert

Institute of General Mechanics, RWTH Aachen University, Germany

ARTICLE INFO

Article history:
Received 1 December 2015
Received in revised form 7 July 2016
Accepted 11 July 2016
Available online 16 July 2016

Keywords:
Hydraulic fracture
Phase-field modeling
PFM
Porous media
TPM

ABSTRACT

Continuum porous media theories, extended by a diffusive phase-field modeling (PFM) approach, introduce a convenient and efficient tool to the simulation of hydraulic fracture in fluid-saturated heterogeneous materials. In this, hydraulic- or tension-induced fracture occurs in the solid phase. This leads to permanent local changes in the permeability, the volume fractions of the constituents as well as the interstitial-fluid flow. In this work, the mechanical behaviors of the multi-field, multi-phase problem of saturated porous media, such as the pore-fluid flow and the solid-skeleton deformation, are described using the macroscopic Theory of Porous Media (TPM). To account for crack nucleation and propagation in the sense of brittle fracture, the energy-minimization-based PFM procedure is applied, which approximates the sharp edges of the crack by a diffusive transition zone using an auxiliary phase-field variable. Furthermore, the PFM can be implemented in usual continuum finite element packages, allowing for a robust solution of initial-boundary-value problems (IBVP). For the purpose of validation and comparison, simulations of a two-dimensional IBVP of hydraulic fracture are introduced at the end of this research paper.

1. Introduction

Prediction and understanding of fracture of solid and porous materials is a very important and challenging subject in engineering and material science, which attracted a lot of theoretical and numerical studies in the last few decades. In case of fluid-saturated porous materials, the focus is mainly on hydraulic fracture caused by a pressurized pore fluid and leading to damage of the solid matrix. This topic finds applications, for instance, in the field of mining and petroleum engineering when talking about fracking of shale rocks to obtain shale gas, in geomechanics when studying the stability of dams, or in biomechanics when intervertebral disc herniation might occur due to a pressurized nucleus pulposus.

The underlying modeling of hydraulic fracture proceeds from a brittle material behavior and uses the phase-field modeling (PFM) approach. The PFM approximates the sharp edges of the crack by a diffusive or smeared-out interface. Thus, after occurrence of the fracture, no discontinuity in the geometry or the finite-element mesh takes place. In particular, an auxiliary scalar field variable (called the phase-field variable) is introduced to distinguish between the broken and the intact solid material. Additionally, a length scale parameter defines the width of the transition zone at the diffusive edge of the crack.

To give an overview about the development of the PFM, Griffith [14] introduced in 1921 an elastic-energy-based approach to describe brittle fracture of elastic solids such as in glass. Thus, cracks propagate if the energy release rate reaches a critical value. This approach has been substantially extended by Irwin [17] by advancing the strain-energy release rate and the fracture toughness concept that introduced a new criterion to determine the initiation of cracks. In physics, the idea of diffuse interfaces has been used by, e.g. Cahn and Hilliard [8] to describe the interfaces in a heterogeneous system by a fourth order partial differential equation. A link between fracture and diffusive interfaces has been proposed in Bourdin et al. [6] in an analogy to the modeling of image segmentation problems by Mumford and Shah [34]. Within a variational framework, essential advances have been made by, e.g., Francfort and Marigo [13], Bourdin et al. [5], Miehe et al. [29] and Kuhn and Müller [19], which allowed to simulate multi-dimensional, mixed-mode fracture scenarios including dynamic effects and crack branching. To give the PFM parameters a realistic meaning and physical estimation, Patil et al. [36] recently introduced a comparative study between the physically-motivated molecular dynamics (MD) simulations of cracks on the nano-scale and the continuum PFM scheme. Considering multi-phase, fluid-saturated porous materials, the aforementioned PFM is applied to

* Corresponding author.
E-mail address: heider@iam.rwth-aachen.de (Y. Heider).

http://dx.doi.org/10.1016/j.mechrescom.2016.07.002
0093-6413/

simulate cracks in the solid phase that could be induced by the increase of the pore pressure, cf. Markert and Heider [26]. This leads, however, to permanent changes of the local physics of the problem, such as of the volume fractions and the permeability, which will be discussed in more details in the following sections.

In the related literature, different approaches for the modeling of hydraulic fracture in saturated porous materials can be found. Based on a cohesive-zone model, a micro-macro-scale approach has been considered by Réthoré et al. [39,40] and Kraaijeveld and Huyghe [18] to treat the change of the flow type in the cracked region. In Secchi and Schrefler [42] and Secchi et al. [43], the modeling of pressure-induced fracture in porous materials is carried out using a cohesive, discrete crack model, which requires continuous updating of the mesh as the crack tip advances, so that cracks can propagate in arbitrary directions. The model described in Li et al. [22] for hydraulic fracture simulation is based on an elastic damage constitutive law with residual strength, where damage can occur under tension or shear. In this, experimental data have also been introduced to validate the numerical results. Recently, a phase-field approach for hydraulic fracture in porous media based on Biot's equations has been investigated by Mikelić et al. [31,32], Lee et al. [21] and Miehe et al. [30]. This allowed to describe the different features of hydraulic fracture in 2D and 3D settings and to apply advanced numerical schemes and algorithms.

The numerical simulation of hydraulic fracture in this contribution is introduced within a continuum-mechanical framework using the Theory of Porous Media (TPM) extended by the diffusive PFM. In the TPM, a macroscopic description of general immiscible fluid-saturated aggregates is introduced, where the individual constituents (here: solid and fluid) are considered to be in a state of ideal disarrangement over a homogenized representative volume element (RVE) in the sense of superimposed and interacting continua, cf. de Boer and Ehlers [9,11] for detailed references. The present work also considers the change of the flow type from Darcy's flow in the porous medium into Stokes-like flow in the cracked region. For the numerical treatment, saturated, materially incompressible porous media are represented by a set of differential-algebraic equations (DAE), which belongs to the class of strongly-coupled problems discussed by, e.g., Felippa et al. [12] and Matthies et al. [28] or more generally by Markert [24,25] and Heider [16]. Applying the PFM to model fracture adds an additional evolution equation for the phase field. Thus, a coupled three-field problem (elasticity, pressure, phase-field) has to be solved, which is demanding in the perspective of the numerical stability.

To give a brief overview, Section 2 describes the basics of the TPM and the extension by the phase-field method, including the concept of volume fractions, saturation as well as the occurrence of the solid matrix crack. Moreover, the kinematics of biphasic continua, the governing balance and constitutive relations, under the assumptions of materially incompressible constituents and linear elastic behavior, are introduced. At the end of this section, the energy formulations of the diffusive porous media fracture and the applied PFM are discussed. Section 3 is concerned with the numerical treatment, such as the derivation of the weak formulations, the spatial discretization using the FEM and the time discretization. The considered formulations are applied in Section 4 to solve a two-dimensional hydraulic fracture problem. This is followed by the conclusions and the outlook in the last section.

2. Theoretical fundamentals

In this section, fundamentals of the multi-phase continuum TPM and its extension to model hydraulic fracture as well as fracture energy formulations are briefly introduced. More information and references about the macroscopic modeling of porous materials could be found in, e.g., [11,27], whereas details and citations related to the fracture energy treatment are given in, e.g., [1,19,26,35,41].

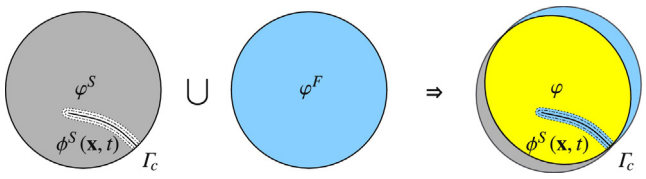

Fig. 1. Schematic illustration of a biphasic solid-fluid body with discontinuity boundary Γ_c representing a crack in the solid matrix, cf. [26].

2.1. Extended multi-phase continuum mechanics

Applying the macroscopic TPM to describe a biphasic porous body consisting of immiscible fluid and solid constituents, the microscopically heterogeneous biphase material is assumed to be in a state of ideal disarrangement over a representative elementary volume (REV). Implementation of a homogenization process to the REV yields a smeared-out continuum φ with overlapped, interacting and statistically distributed solid and fluid aggregates φ^α ($\alpha = S$ for solid phase and $\alpha = F$ for pore-fluid phase). Under the assumption of immiscible aggregates, the volume fraction $n^\alpha := \mathrm{d}v^\alpha/\mathrm{d}v$ of φ^α is defined as the ratio of the partial volume element $\mathrm{d}v^\alpha$ to the total volume element $\mathrm{d}v$ of φ. The saturation constraint for the case of a fully saturated medium is given by

$$\sum_\alpha n^\alpha = n^S + n^F = 1 \quad \text{with} \quad \begin{cases} n^S: & \text{solidity}, \\ n^F: & \text{porosity}, \end{cases} \tag{1}$$

and is assumed to be satisfied during the whole deformation process in the sense of an algebraic side condition. By means of n^α, two density functions can further be defined, namely a material (effective or intrinsic) density $\rho^{\alpha R} := \mathrm{d}m^\alpha/\mathrm{d}v^\alpha$ and a partial density $\rho^\alpha := \mathrm{d}m^\alpha/\mathrm{d}v$, with $\mathrm{d}m^\alpha$ being the local mass element of φ^α.

In porous media theories, such as the TPM or Biot's Theory, both n^S and n^F are supposed to be smaller than 1 and greater than 0 ($0 < n^\alpha < 1$), and the fluid flow is governed by some porous media filter law, such as the Darcy or Forchheimer law, cf. [23]. In the presence of a fracture, the cracked region is assumed to be free of the solid phase ($n^S = 0$) and completely filled with the fluid ($n^F = 1$). Therefore, it is conceivable to treat the fluid flow in the fully saturated crack in the sense a of Stokes's flow. For illustration, Fig. 1 schematically shows an arbitrary saturated porous body $\mathcal{B}$ with external boundary $\mathcal{S}$ and internal discontinuity boundary Γ_c in the solid phase. The occurring discontinuity is treated as a diffusive crack and is governed by the phase-field variable $\phi^S(\mathbf{x}, t)$ as a function of space $\mathbf{x}$ and time t, which serves continuously to distinguish between the state of a cracked solid phase ($\phi^S = 0$) and the state of an intact solid phase ($\phi^S = 1$).

To describe the motion of a multiphase body within a continuum mechanical framework, the individual constituents φ^α are considered to follow unique states of motion, see, e.g., [7,15]. Thus, starting from different positions $\mathbf{X}_\alpha$ in the reference configuration, each constituent has an individual Lagrangian (material) motion function $\boldsymbol{\chi}_\alpha$ and has its own velocity field, viz.:

$$\mathbf{x} = \boldsymbol{\chi}_\alpha(\mathbf{X}_\alpha, t) \Leftrightarrow \mathbf{X}_\alpha = \boldsymbol{\chi}_\alpha^{-1}(\mathbf{x}, t), \quad \mathbf{v}_\alpha := \overset{\prime}{\mathbf{x}}_\alpha = \frac{\mathrm{d}_\alpha \mathbf{x}}{\mathrm{d}t}. \tag{2}$$

Therein, $\boldsymbol{\chi}_\alpha^{-1}$ represents the unique inverse (Eulerian or spatial) motion function and

$$(\,\cdot\,)'_\alpha := \frac{\mathrm{d}_\alpha(\,\cdot\,)}{\mathrm{d}t} = \frac{\partial(\,\cdot\,)}{\partial t} + \mathrm{grad}(\,\cdot\,)\cdot\mathbf{v}_\alpha \tag{3}$$

indicates the material time derivative of an arbitrary quantity $(\cdot)$ following the motion of φ^α with $\mathrm{grad}(\cdot) := \partial(\cdot)/\partial\mathbf{x}$. In the following,

a Lagrangian approach is applied for the description of the solid-phase motion via the solid displacement $\mathbf{u}_S$ and velocity $\mathbf{v}_S$. For the pore-fluid flow, the motion is described either by an Eulerian description using the fluid velocity $\mathbf{v}_F$ or by a modified Eulerian setting via the seepage velocity $\mathbf{w}_F$. In particular, we have

$$\mathbf{u}_S = \mathbf{x} - \mathbf{X}_S, \quad \mathbf{v}_S = (\mathbf{u}_S)'_S, \quad \mathbf{w}_F = \mathbf{v}_F - \mathbf{v}_S. \tag{4}$$

It is worth mentioning that in the later discussion, $\mathbf{v}_F$ is adopted as the primary unknown for the pore-fluid motion rather than $\mathbf{w}_F$. This choice coincides with the idea of changing flow in the cracked region from Darcy to Stokes, as no seepage velocity exists in the Stokes's flow approach. Following this, the essential kinematic relation within the geometric linear framework is the linearized small solid strain $\boldsymbol{\varepsilon}_S$, which is expressed as

$$\boldsymbol{\varepsilon}_S = \frac{1}{2}(\operatorname{grad}\mathbf{u}_S + \operatorname{grad}^T\mathbf{u}_S). \tag{5}$$

In addition to the aforementioned variables, two more primary variables emerge in the balance relations, namely, the pore-fluid pressure $p = p(\mathbf{x}, t)$ accounting for the interaction between the solid and fluid phases, and the phenomenological phase-field variable $\phi^S = \phi^S(\mathbf{x}, t)$ that indicates the crack location.

To simplify the balance relations of porous media, a number of assumptions are required such as excluding of the dynamic effects (quasi-static case), the thermal effects as well as any mass production. Additionally, the treatment proceeds from materially incompressible constituents ($\rho^{\alpha R} = \text{const.}$). Thus, the arising purely mechanical model with $\alpha = \{S, F\}$ is governed by the following strongly coupled constituent balance equations:

- Partial mass balance $\longrightarrow$ partial volume balance:

$$0 = (\rho^\alpha)'_\alpha + \rho^\alpha \operatorname{div}\mathbf{v}_\alpha \longrightarrow 0 = (n^\alpha)'_\alpha + n^\alpha \operatorname{div}\mathbf{v}_\alpha \tag{6}$$

- Partial momentum balance:

$$\mathbf{0} = \operatorname{div}\mathbf{T}^\alpha + \rho^\alpha\mathbf{b} + \hat{\mathbf{p}}^\alpha. \tag{7}$$

Herein, $\operatorname{div}(\cdot)$ is the divergence operator, $\mathbf{T}^\alpha = (\mathbf{T}^\alpha)^T$ is the symmetric partial Cauchy stress assuming non-polar constituents (referred to $\boldsymbol{\sigma}^\alpha$ within the small strain treatment), $\mathbf{b}$ is the mass-specific body force acting on the overall aggregate, and $\hat{\mathbf{p}}^\alpha$ denotes the direct momentum production (local interaction force) between φ^S and φ^F. Due to the overall conservation of momentum, $\hat{\mathbf{p}}^S + \hat{\mathbf{p}}^F = \mathbf{0}$ must hold.

Eq. $(6)_2$ with $\alpha = S$ yields the solid volume fraction, which can analytically be integrated over time to get an explicit relation of the solid volume fraction (solidity) n^S (see Appendix A). Thus, having n^S_{0S} as the initial solidity related to the undeformed and undamaged state, and $n^S_\phi := \phi^S n^S_{0S}$ (with $n^S_\phi = n^S_{0S}$ if $\phi^S = 1$) is the initial solidity of the undeformed but possibly cracked state of the porous material, one directly obtains the current solidity as a secondary variable as

$$(n^S)'_S = -n^S \operatorname{div}\mathbf{v}_S \longrightarrow n^S = n^S_\phi \det\mathbf{F}_S^{-1} \tag{8}$$

with $\mathbf{F}_S = \partial\mathbf{x}/\partial\mathbf{X}_S$ being the solid deformation gradient. Eq. $(8)_2$ considers that inside the crack there is no solid phase, i.e., $\phi^S = 0$ yields $n^S = 0$ and $n^F = 1$. Additionally, it takes into account the deterioration of n^S in the crack diffusive interface where $0 < \phi^S < 1$. In the stress-free state (after unloading), the crack cannot be recovered and, thus, it remains free of the solid phase, which is assured in the modeling by use of Eq. $(8)_2$. In other words, n^S_ϕ assists the changes of the reference configuration if a non-healing crack has developed. Following this, n^S can be further simplified within the small strain approach, yielding:

$$n^S \approx n^S_\phi(1 - \operatorname{div}\mathbf{u}_S) \quad \text{with} \quad 0 \le n^S < 1. \tag{9}$$

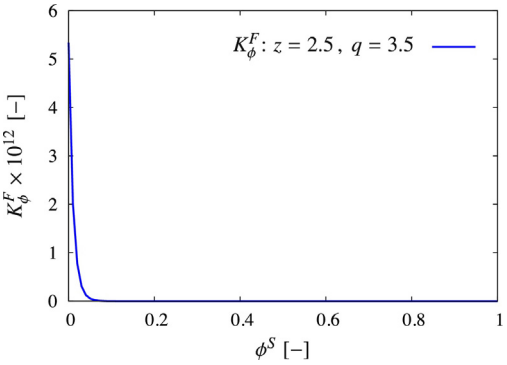

Fig. 2. Increase of the permeability by increasing of K^F_ϕ in connection with ϕ^S decrease (Here: $z = 2.5$, $q = 3.5$), see [37].

2.1.1. *Effective stresses and permeability formulation*

The stress state in a material point of a fluid-saturated porous medium consists of two coupled components: An 'extra' or 'effective' stress indicated by the subscript $(\cdot)_E$, and a weighted pore-fluid pressure term, cf. [3,10] for a historical review of the effective stresses principle. Thus, $\boldsymbol{\sigma}^\alpha$ and $\hat{\mathbf{p}}^\alpha$ with $\alpha = \{S, F\}$ (see Eq. (7)) can be expressed as

$$\begin{aligned} &\boldsymbol{\sigma}^S = \boldsymbol{\sigma}^S_E - n^S p\mathbf{I}, \quad \boldsymbol{\sigma}^F = \boldsymbol{\sigma}^F_E - n^F p\mathbf{I}, \\ &\mathbf{p}^F = \mathbf{p}^F_E + p \operatorname{grad} n^F. \end{aligned} \tag{10}$$

For a possibly linear elastic solid phase, the related effective stress $\boldsymbol{\sigma}^S_E$ is given as the derivative of the free energy function Ψ^S_{el} with respect to the strain $\boldsymbol{\varepsilon}_S$, as will be shown in details in Section 2.2. For a materially incompressible pore fluid and isotropic permeability tensor $\mathbf{K}^F$, the constitutive equation of the interaction force $\mathbf{p}^F$ between the permeating fluid and the solid skeleton can be expressed as

$$\mathbf{p}^F_E = -(n^F)^2(\mathbf{K}^F)^{-1}\mathbf{w}_F \quad \text{with} \quad \mathbf{K}^F := K^F\mathbf{I} = \frac{k^F}{\gamma^{FR}}\mathbf{I}, \tag{11}$$

where k^F is the hydraulic conductivity in [length/time] with initial value k^F_0, and $\gamma^{FR} = \rho^{FR}g$ is the effective fluid weight with g as the gravitational acceleration. In this contribution, the following relation of the permeability K^F is adopted, which considers both, the influence of solid matrix deformation through $K^F_{\mathbf{u}}$ and the development of the crack through K^F_ϕ:

$$K^F = \frac{k^F_0}{\gamma^{FR}} \underbrace{\operatorname{Exp}[(z(1-\phi^S))^q]}_{K^F_\phi} \underbrace{\left[\frac{1 - n^S_\phi(1 - \operatorname{div}\mathbf{u}_S)}{(1 - n^S_\phi)(1 - \operatorname{div}\mathbf{u}_S)}\right]^\kappa}_{K^F_{\mathbf{u}}}. \tag{12}$$

The parameter $\kappa \ge 0$ influences the deformation dependency of the permeability, where $K^F_{\mathbf{u}}$ is a reformulation of the permeability given in [23]. Moreover, $\{z, q\} \ge 0$ are additional material parameters that govern the increase of K^F depending on ϕ^S. The formulation of K^F_ϕ is adopted from [37] within a diffusive damage modeling, which considers the increase of the permeability on the macro-crack edges of a porous concrete under tension due to the development of micro cracks. In the stress-free state, the crack cannot be recovered, but $\mathbf{u}_S = \mathbf{0}$ and $K^F_{\mathbf{u}} = 1$. Thus, the increased permeability in the crack is realized through the term K^F_ϕ. For illustration, Fig. 2 depicts the increase of K^F_ϕ as ϕ^S decreases. Furthermore, Eqs. (11) and (12) show that the interaction force $\mathbf{p}^F_E$ decreases gradually as the crack is initiated and K^F increases, where for a complete crack the only medium is assumed to be fluid. A residual small value of $\mathbf{p}^F_E$ assists, however, the numerical stability of the calculation.

The pore fluid is considered Newtonian, incompressible (ρ^{FR} = const.) and isotropic. Thus, the effective fluid viscous stress can for simplicity be expressed as

$$\boldsymbol{\sigma}_E^F = \mu^F(\operatorname{grad}\mathbf{v}_F + \operatorname{grad}^T\mathbf{v}_F), \tag{13}$$

with $\mu^F := n^F\mu^{FR} > 0$ being the partial shear or dynamic viscosity and μ^{FR} is the effective dynamic viscosity of the fluid.

2.2. PFM formulation

Within the framework of brittle fracture as given in, e.g., [13,14], the global potential energy function $\mathcal{F}$ of a cracked linear elastic and isotropic body can be defined as the sum of the elastic strain energy $\overline{\Psi}^S_{\text{el}}$ integrated over the whole spatial domain Ω, and the critical fracture energy (crack resistance) G_c (equal to the energy required to create a unit area of fracture surface) integrated along the crack path Γ_c;

$$\mathcal{F}(\boldsymbol{\varepsilon}_S, \Gamma_c) = \int_\Omega \overline{\Psi}^S_{\text{el}}(\boldsymbol{\varepsilon}_S)\,\mathrm{d}v + \int_{\Gamma_c} G_c\,\mathrm{d}\Gamma_c. \tag{14}$$

For a plausible numerical implementation, the phenomenological phase-field variable ϕ^S is incorporated, which approximates the crack-material sharp interface by a diffusive transition zone. Thus, the potential energy function can be rewritten as an integration over the whole body (cf. [4,5,13,19,20,26,45]) with $\Psi = \Psi^S_{\text{el}} + \Psi^S_{\text{crack}}$ as

$$\mathcal{F}(\boldsymbol{\varepsilon}_S, \phi^S, \operatorname{grad}\phi^S) = \int_\Omega [\Psi^S_{\text{el}}(\boldsymbol{\varepsilon}_S, \phi^S) + \Psi^S_{\text{crack}}(\phi^S, \operatorname{grad}\phi^S)]\mathrm{d}v. \tag{15}$$

The initiation of fracture is associated with an elastic energy degradation, which is assumed to occur only under tension and shear and not under compression in our treatment. Thus, the elastic volumetric energy is split into a positive (includes tension and shear) and a negative (includes compression) part, which allows introducing a formulation based on the strain history in order to avoid crack healing in the numerical calculation, see, e.g., [19,29]. In particular,

$$\begin{aligned}\Psi^S_{\text{el}}(\boldsymbol{\varepsilon}_S, \phi^S) &= [(1-\eta)(\phi^S)^2 + \eta]\Psi^{S+}_{\text{el}} + \Psi^{S-}_{\text{el}} \\ &= [(1-\eta)(\phi^S)^2 + \eta]\left[\frac{1}{2}B^S[\operatorname{tr}^+(\boldsymbol{\varepsilon}_S)]^2 + \mu^S\boldsymbol{\varepsilon}^D_S\cdot\boldsymbol{\varepsilon}^D_S\right] \\ &\quad + \frac{1}{2}B^S[\operatorname{tr}^-(\boldsymbol{\varepsilon}_S)]^2.\end{aligned} \tag{16}$$

with $B^S := \mu^S + (2/3)\lambda^S$ being the bulk modulus of the porous solid matrix, μ^S and λ^S are the macroscopic Lamé constants, $\operatorname{tr}(\boldsymbol{\varepsilon}_S) := \boldsymbol{\varepsilon}_S\cdot\mathbf{I} = \operatorname{div}\mathbf{u}_S$ is the trace of the strain tensor $\boldsymbol{\varepsilon}_S$ and $\boldsymbol{\varepsilon}^D_S$ is the elastic deviatoric strain tensor. Additionally, η is a small positive parameter, which serves as a residual stiffness, used for numerical stability purposes, see [19,31]. $\operatorname{tr}^+(\boldsymbol{\varepsilon}_S) = \max\{0, \operatorname{tr}(\boldsymbol{\varepsilon}_S)\}$ and $\operatorname{tr}^-(\boldsymbol{\varepsilon}_S) = \min\{0, \operatorname{tr}(\boldsymbol{\varepsilon}_S)\}$ are the positive and the negative traces of the strain tensor, respectively. Thereafter, the effective stress tensor is defined as the variational derivative of the strain energy function with respect to the strain tensor:

$$\begin{aligned}\boldsymbol{\sigma}^S_E &= \frac{\partial\Psi^S_{\text{el}}(\boldsymbol{\varepsilon}_S, \phi^S)}{\partial\boldsymbol{\varepsilon}_S} \\ &= [(1-\eta)(\phi^S)^2 + \eta][B^S\operatorname{tr}^+(\boldsymbol{\varepsilon}_S)\mathbf{I} + 2\mu^S\boldsymbol{\varepsilon}^D_S] + B^S\operatorname{tr}^-(\boldsymbol{\varepsilon}_S)\mathbf{I}.\end{aligned} \tag{17}$$

The fracture energy as a function of the phase field and its gradient can be expressed as

$$\begin{aligned}\Psi^S_{\text{crack}}(\phi^S, \operatorname{grad}\phi^S) &= G_c\gamma(\phi^S, \operatorname{grad}\phi^S) \\ &= G_c\left[\frac{1}{4\epsilon}(1-\phi^S)^2 + \epsilon|\operatorname{grad}\phi^S|^2\right]\end{aligned} \tag{18}$$

with ϵ being the internal length (regularization parameter), that defines the width of the transition zone between the cracked and the uncracked zones. This parameter should be chosen reasonably small in order to get good approximation of the sharp crack edges. However, a very small value of ϵ should be avoided as it requires a very fine FE mesh in the cracked edges (see, [2,36] for a thoroughly discussion). Moreover, $\gamma(\phi^S, \operatorname{grad}\phi^S)$ is the crack density function per unit volume, cf. [29]. The phase-field evolution is derived using the Allen–Cahn model, which describes the process of phase separation (here crack formation) via a reaction-diffusion equation:

$$\begin{aligned}\frac{\mathrm{d}\phi^S(\mathbf{x}, t)}{\mathrm{d}t} &= (\phi^S)'_S = -M\frac{\partial\Psi}{\partial\phi^S} \\ &= -M[2(1-\eta)\phi^S\Psi^{S+}_{\text{el,max}} - \frac{G_c}{2\epsilon}(1-\phi^S) \\ &\quad - 2G_c\epsilon(\operatorname{div}\operatorname{grad}\phi^S)]\end{aligned} \tag{19}$$

with $M > 0$ being a scalar-valued kinetic parameter related to the interface mobility (time dependency), which is adopted in the underlying treatment as a constant yielding a standard Ginzburg–Landau evolution equation, see [19,30,33]. For rate-independent settings, $M \to \infty$ yielding $\partial\Psi/\partial\phi^S = 0$, which is not considered in this work. A smaller value of M leads to a slower crack propagation. Therefore, M has to be chosen sufficiently small, so that the crack propagation speed is realistic and the fluid has time fill the crack. However, too small M should also be avoided as it leads to undesired local energy dissipation as will be shown in the numerical example.

In Eq. (19), $\Psi^{S+}_{\text{el,max}}$ represents the maximum positive elastic strain energy density defined as

$$\Psi^{S+}_{\text{el,max}} := \max_{\tau\in[0,t]}\Psi^{S+}_{\text{el}}(\boldsymbol{\varepsilon}_S(\mathbf{x}, \tau)), \tag{20}$$

which is introduced following [29] to prevent crack healing and to assure the irreversibility of the phase-field variable (i.e. $(\phi^S)'_S \le 0$) upon loading/unloading processes.

2.3. Governing PDEs

The governing partial differential equations (PDE) with primary unknowns $\{\mathbf{u}_S, \mathbf{v}_F, p, \phi^S\}$ are summarized as follows:

- Overall momentum balance:

$$\mathbf{0} = \operatorname{div}\underbrace{[\boldsymbol{\sigma}^S_E(\mathbf{u}_S, \phi^S) + \boldsymbol{\sigma}^F_E(\mathbf{v}_F) - p\,\mathbf{I}]}_{\boldsymbol{\sigma}} + \rho\mathbf{b}. \tag{21}$$

- Momentum balance of the pore fluid:

$$\mathbf{0} = \operatorname{div}[\boldsymbol{\sigma}^F_E(\mathbf{v}_F)] - n^F\operatorname{grad}p + \rho^F\mathbf{b} - (n^F)^2(\mathbf{K}^F)^{-1}(\mathbf{v}_F - \mathbf{v}_S). \tag{22}$$

- Overall volume balance:

$$0 = \operatorname{div}(n^S\mathbf{v}_S + n^F\mathbf{v}_F) - \alpha\operatorname{div}\operatorname{grad}p. \tag{23}$$

- Phase-field evolution equation:

$$(\phi^S)'_S = -M\left[2(1-\eta)\phi^S\Psi^{S+}_{\text{el,max}} - \frac{G_c}{2\epsilon}(1-\phi^S) - 2G_c\epsilon(\operatorname{div}\operatorname{grad}\phi^S)\right]. \tag{24}$$

In Eq. (23), α is a small stabilizing parameter controlling the influence of the Laplacian term div grad p as a materially-incompressible fluid is considered. In fact, this is comparable to the pressure-stabilization or quasi-compressibility methods used in computational fluid dynamics (CFD), cf. [38]. The underlying formulations (21)–(24) take into account the change of the flow from Darcy to Stokes-like in the cracked region. In particular, for a cracked region, which is fully filled with fluid, $n^F = 1$, $n^S = 0$ and $\phi^S = 0$. Thus, the Stokes's equations are automatically recovered, where Eq. (21) or (22) yields the fluid momentum balance and Eq. (23) yields the continuity equation. In particular, the resulting Stokes-like governing equations in the cracked region with primary unknowns $\{\mathbf{v}_F, p\}$ read:

- Fluid momentum balance: results from Eq. (21)

$$\mathbf{0} = \operatorname{div}\left[\cancelto{\approx 0}{\boldsymbol{\sigma}_E^S(\mathbf{u}_S, \phi^S)} + \boldsymbol{\sigma}_E^F(\mathbf{v}_F) - p\,\mathbf{I}\right] + \cancelto{\rho^F}{\phi^F}\mathbf{b}, \tag{25}$$

or from Eq. (22)

$$\mathbf{0} = \operatorname{div}\left[\boldsymbol{\sigma}_E^F(\mathbf{v}_F)\right] - n^F \operatorname{grad} p + \rho^F\,\mathbf{b} \cancelto{\approx 0}{- (n^F)^2 (\mathbf{K}^F)^{-1}(\mathbf{v}_F - \mathbf{v}_S)}. \tag{26}$$

- Continuity equation: results from Eq. (23)

$$0 = \operatorname{div}(\cancelto{0}{n^S}\mathbf{v}_S + \cancelto{1}{n^F}\mathbf{v}_F) - \alpha \operatorname{div} \operatorname{grad} p. \tag{27}$$

3. FE implementation

The finite element method (FEM) is applied for the numerical solution of initial-boundary value problems (IBVP) of porous media fracture. In the FEM, Eqs. ((21)–(24)) are weighted by independent test functions and integrated over the spatial domain Ω to derive the weak formulation. Moreover, the product rule and the Gaussian integral theorem are applied to get the boundary terms $\Gamma = \partial\Omega$, where Γ is split into Dirichlet (essential) and Neumann (natural) boundaries (see, e.g. [16,27,46] for detailed discussion). In particular, the overall aggregate momentum balance in a weak form reads

$$\int_\Omega \operatorname{grad}\delta\mathbf{u}_S \cdot \boldsymbol{\sigma}\,\mathrm{d}v - \int_{\Gamma_\mathbf{t}} \delta\mathbf{u}_S \cdot \bar{\mathbf{t}}\,\mathrm{d}a - \int_\Omega \delta\mathbf{u}_S \cdot \rho\mathbf{b}\,\mathrm{d}v = 0 \tag{28}$$

with $\delta\mathbf{u}_S$ being the test function corresponding to the primary variable $\mathbf{u}_S$ and $\bar{\mathbf{t}} = \boldsymbol{\sigma}\mathbf{n}$ is the external load vector acting on the Neumann boundary $\Gamma_\mathbf{t}$ of the overall aggregate with outward-oriented unit surface normal $\mathbf{n}$. The weak form of the fluid momentum balance can be expressed as

$$\int_\Omega \operatorname{grad}\delta\mathbf{v}_F \cdot \boldsymbol{\sigma}_E^F\,\mathrm{d}v - \int_\Omega \operatorname{div}\delta\mathbf{v}_F n^F p\,\mathrm{d}v - \int_{\Gamma_\mathbf{t}^F} \delta\mathbf{v}_F \cdot \bar{\mathbf{t}}^F\,\mathrm{d}a + + \int_\Omega \delta\mathbf{v}_F \cdot [-\rho^F\mathbf{b} + (n^F)^2(\mathbf{K}^F)^{-1}(\mathbf{v}_F - \mathbf{v}_S)]\mathrm{d}v = 0, \tag{29}$$

where $\delta\mathbf{v}_F$ is the test function corresponding to the primary variable $\mathbf{v}_F$. Moreover, $\bar{\mathbf{t}}^F = (\boldsymbol{\sigma}_E^F - n^F p\mathbf{I})\,\mathbf{n}$ is the external fluid load vector acting on $\Gamma_\mathbf{t}^F$. For a cracked medium with $\phi^S = 0$ and $\eta \ll 1$, the boundary terms in Eqs. (28) and (29) read $\bar{\mathbf{t}} \approx \bar{\mathbf{t}}^F = (\boldsymbol{\sigma}_E^F - p\mathbf{I})\mathbf{n}$. The overall aggregate volume balance in weak form reads

$$\int_\Omega \delta p \operatorname{div}\mathbf{v}_S\,\mathrm{d}v - \int_\Omega \operatorname{grad}\delta p \cdot n^F(\mathbf{v}_F - \mathbf{v}_S)\,\mathrm{d}v + + \alpha\int_\Omega \operatorname{grad}\delta p \cdot \operatorname{grad}\delta p\,\mathrm{d}v + \int_{\Gamma_v} \delta p\bar{v}\,\mathrm{d}a = 0 \tag{30}$$

with δp being the test function related to the primary variable p and $\bar{v} = n^F\mathbf{w}_F \cdot \mathbf{n}$ denotes the volume efflux of the fluid draining through the Neumann boundary Γ_v. For a cracked medium, this boundary term becomes $\bar{v} \approx \mathbf{v}_F \cdot \mathbf{n}$. Similarly to [19], the weak formulation of the phase-field evolution equation (24) can be expressed as

$$\int_\Omega \delta\phi^S \left[\frac{(\phi^S)'_S}{M} + 2(1-\eta)\phi^S\Psi^{S+}_{\mathrm{el,max}} - \frac{G_c}{2\epsilon}(1-\phi^S)\right]\mathrm{d}v + \int_\Omega \operatorname{grad}\delta\phi^S \cdot (2G_c\epsilon)\operatorname{grad}\phi^S\mathrm{d}v - \int_{\Gamma_\phi} \delta\phi^S(2G_c\epsilon)\operatorname{grad}\phi^S \cdot \mathbf{n}\,\mathrm{d}a = 0 \tag{31}$$

with $\delta\phi^S$ being the test function related to ϕ^S and Γ_ϕ is the corresponding Neumann boundary.

For the spatial semi-discretization using the Bubnov–Galerkin procedure and having $\mathbf{u} := [\mathbf{u}_S\ \mathbf{v}_F\ p\ \phi^S]^T$, the continuous control space Ω is subdivided into N_e finite elements yielding an approximate discrete domain Ω^h, on which the following discrete trial and test functions are defined:

$$\mathbf{u}(\mathbf{x}, t) \approx \mathbf{u}^h(\mathbf{x}, t) = \bar{\mathbf{u}}^h(\mathbf{x}, t) + \sum_{i=1}^{N_\mathbf{u}} \boldsymbol{N}_{\mathbf{u}(i)}(\mathbf{x})\,\mathbf{u}_{(i)}(t),$$

$$\delta\mathbf{u}^h(\mathbf{x}) = \sum_{i=1}^{N_\mathbf{u}} \boldsymbol{N}_{\mathbf{u}(i)}(\mathbf{x})\delta\mathbf{u}_{(i)}. \tag{32}$$

In this, $\bar{\mathbf{u}}^h$ refers to the approximated Dirichlet boundary conditions of the considered problem, $N_\mathbf{u}$ denotes the number of FE nodes used for the approximation of the respective fields in $\mathbf{u}$ and the corresponding test functions $\delta\mathbf{u}$, and $\boldsymbol{N}_{\mathbf{u}(i)}$ represents the global basis functions at node i, which depend only on the spatial position $\mathbf{x}$. Additionally, $\mathbf{u}_{(i)} := [\mathbf{u}_S\ \mathbf{v}_F\ \mathbf{p}\ \boldsymbol{\phi}^S]^T$ refers to the time-dependent nodal coefficients of the solid displacement, the fluid velocity, the fluid pressure and the phase-field variable, respectively. $\delta\mathbf{u}_{(i)}$ represents the nodal values of the test functions $\delta\mathbf{u}^h$. Applying the spatial discretization to Eqs. (28)–(31) yields a coupled, space-discrete PDE system, which can be written in an abstract form as

$$\begin{bmatrix} \boldsymbol{G}^h_{TPM}(t, \mathbf{y}, (\mathbf{y})'_S; \boldsymbol{\phi}^S) \\ \boldsymbol{G}^h_{PFM}(t, \boldsymbol{\phi}^S, (\boldsymbol{\phi}^S)'_S; \mathbf{y}) \end{bmatrix} \overset{!}{=} \mathbf{0} \tag{33}$$

with $\mathbf{y} := \mathbf{y}(t) = [\mathbf{u}_S\,\mathbf{v}_F\,\mathbf{p}]^T$. In Eq. (33), $\boldsymbol{G}^h_{TPM}$ represents the space-discrete, strongly coupled TPM problem, which results from Eqs. (28)–(30), whereas $\boldsymbol{G}^h_{PFM}$ is the space-discrete phase-field evolution equation resulting from Eq. (31). The time integration of the problem is carried out using a combination of monolithic and staggered solution schemes. In particular, the coupled problem $\boldsymbol{G}^h_{TPM}$ is discretized in the first step in time using the monolithic 2nd-order Backward Difference Formula (BDF2) scheme and considering $\boldsymbol{\phi}^S$ as history variable. In the second step, $\boldsymbol{G}^h_{PFM}$ is solved in time using the BDF scheme and considering $\mathbf{y}$ as known values to obtain the updated $\boldsymbol{\phi}^S$. In other words, the staggered strategy reflects the fact that the mechanical TPM problem drives the phase-field evolution, and thus, the crack.

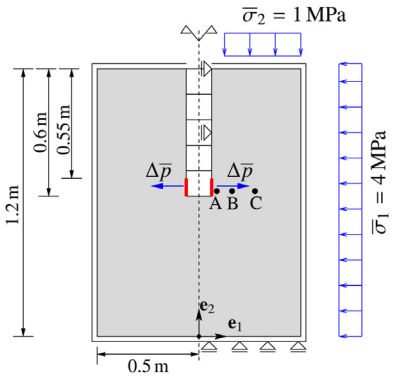

Fig. 3. Geometry and boundary conditions of the symmetric IBVP, cf. [22,26]. In this, the horizontal displacement $\overline{u}_{Sx}$ at the axis of symmetry and the sides of the wellbore and the vertical displacement $\overline{u}_{Sy}$ at the bottom of the sample are set to zero.

4. IBVP of hydraulic fracture

The ability of the discussed model to simulate fluid-pressure-induced crack propagation in a saturated porous material, such as in a rock sample, is introduced in the following numerical example. The implementation is carried out using the Finite Element Method with quadratic shape functions for the primary variables $\{\mathbf{u}_S, \mathbf{v}_F, p, \phi^S\}$. The time integration is performed sequentially in two steps as mentioned in Section 3 using the BDF2 scheme together with time-step adaptivity, where an iteration between the two steps is performed until the desired accuracy is reached.

The settings of the IBVP are mainly adopted from [22] for a laboratory rock sample, and treated for simplicity as a plane-strain problem. To emulate the real in-situ conditions, the sample is subjected to confining stresses as illustrated in Fig. 3 and to an initial pore pressure $\overline{p}_0 = 8.5$ MPa. The boundary conditions of the symmetric boundary-value problem are illustrated in Fig. 3, where the outer boundaries are considered permeable with prescribed pore pressures equal to the initial domain pore pressure $\overline{p}_0$. At the center of the sample, a wellbore of 4 cm diameter is placed, which serves to induce excess pore pressure and, consequently, leads to a hydraulic cracking. The loads are applied in two steps: In the first step ($0 \le t \le 0.2$ s), the initial confining stresses and the pore pressure in the domain and at the boundaries are applied linearly. In the second step ($t > 0.2$ s), the pore pressure at the bottom of the wellbore (see Fig. 3) is increased linearly ($\Delta\overline{p} = 0.67$ MPa/s) until occurrence and propagation of the crack, whereas the confining stresses and the fluid pressure at the outer boundaries are kept constant.

Table 1
Parameters of the numerical example, mostly adopted from [22].

Parameter	Sym.	Val.	Unit
Young's modulus of φ^S	E^S	6×10^3	MPa
Possion's ration of φ^S	ν^S	0.25	–
Effective solid density	ρ^{SR}	2760	kg/m^3
Effective fluid density	ρ^{FR}	1000	kg/m^3
Eff. dyn. fluid viscosity	μ^{FR}	1.002×10^{-3}	N s/m^2
Initial solidity	n^S_{0S}	0.9	–
Initial Darcy permeability	k^F_{0S}	10^{-7}	m/s
Parameter related to $K^F_{\mathbf{u}}$	κ	1	-
Mobility parameter[a]	M	10^{-3}	m^2/N s
Internal length scale[a]	ϵ	10^{-2}	m
Crack resistance	G	1053	J/m^2
Residual stiffness	η	10^{-2}	–

[a] The influence of variation of M and ϵ is studied in this example.

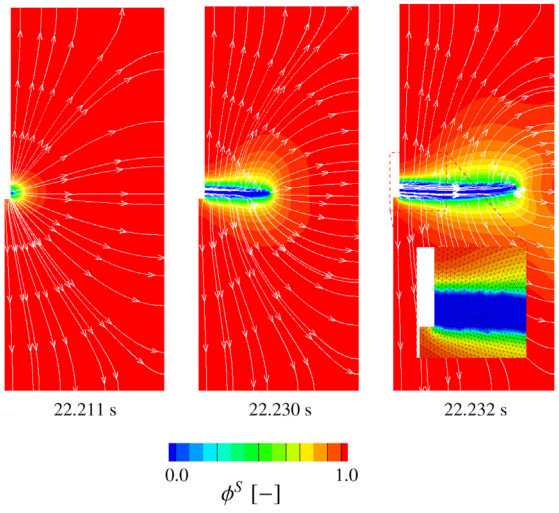

Fig. 4. Phase-field variable contour plots and fluid seepage velocity stream traces during crack propagation for the case of $\Delta\overline{p} = 0.67$ MPa/s, $M = 10^{-3}$ m^2/N s and $\epsilon = 10^{-2}$ m.

The parameters of the assumed brittle porous material are given in Table 1. This includes the parameters of the poroelastic rock and the parameters of the fracture model.

As shown in Figs. 4 and 5, the crack propagates perpendicular to the wellbore, and with this, normal to the maximum stress $\overline{\sigma}_1$ as on the boundaries $\overline{\sigma}_1 > \overline{\sigma}_3$. This result agrees with what has been frequently mentioned in the literature on plane-strain hydraulic fracture as, e.g., in [22,26,43]. The phase-field variable ϕ^S in Fig. 4 is used to indicate the crack path propagation, where it takes the value 0 upon rupture of the solid matrix and 1 for the uncracked state. It is also shown that the fluid stream traces change during crack propagation and demonstrate the fluid flow from the cracked region to the surrounding domain.

The fluid pressure time history at three points A(0.02, 0.63), B(0.08, 0.63) and C(0.17, 0.63) along the crack path is illustrated in Fig. 6. It is clear that a jump of the pore-pressure occurs once the crack reaches points B and C. Thereafter, an oscillation and increase of the pressure takes place until the whole crack propagates.

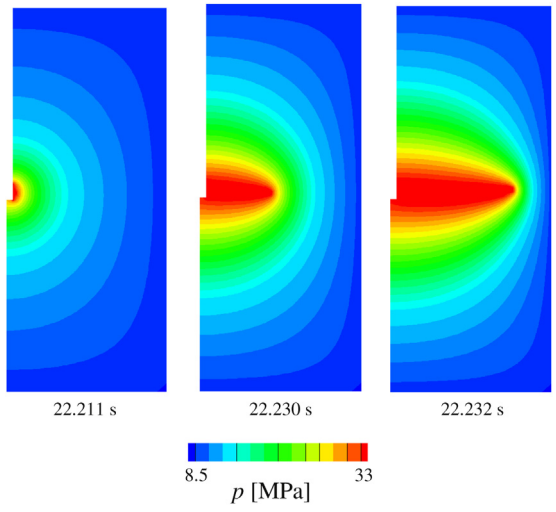

Fig. 5. Fluid pressure contour plots during crack propagation for the case of $\Delta\overline{p} = 0.67$ MPa/s, $M = 10^{-3}$ m^2/N s and $\epsilon = 10^{-2}$ m.

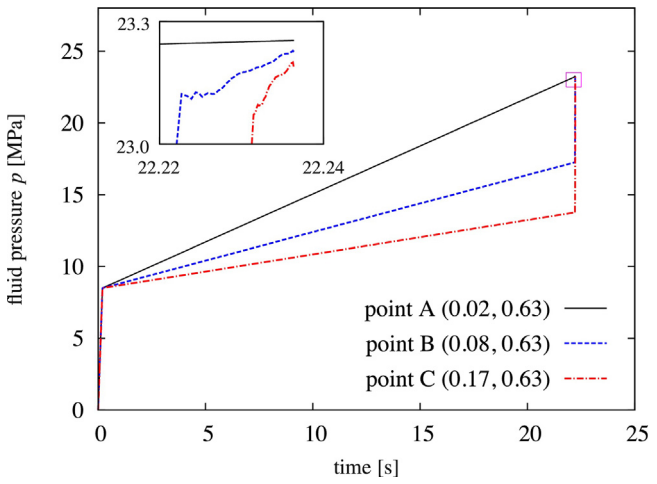

Fig. 6. Fluid pressure time history at points A, B and C at the crack path for the case of $\Delta\overline{p} = 0.67$ MPa/s, $M = 10^{-3}$ m^2/N s and $\epsilon = 10^{-2}$ m.

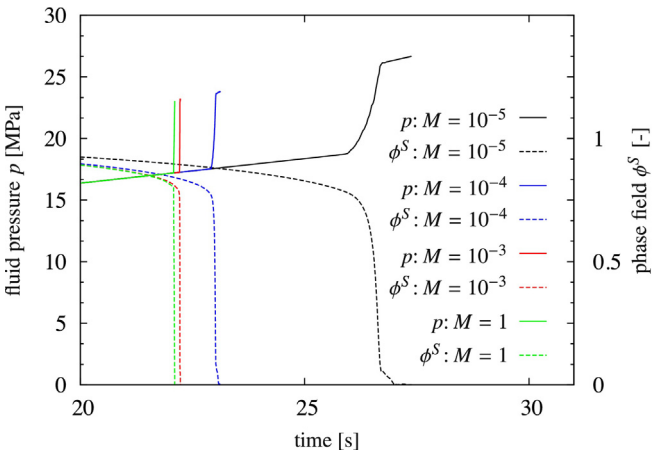

Fig. 8. Fluid pressure and phase-field time histories at point B (0.08, 0.63), which illustrate the effect of the mobility parameter M on the pressure value needed to start the crack and crack speed for the case of $\Delta\overline{p} = 0.67$ MPa/s and $\epsilon = 10^{-2}$ m.

With the given parameters, the crack starts to initiate at time $t_c \approx 22.22$ s, which corresponds to an increase in the fluid pressure in the wellbore of $\Delta\,\overline{p}_c \approx 14.89$ MPa. This value of the underlying 2D model is almost 1.3–1.5 times higher than the cracking pressure values reported in [22], which results from 3D numerical calculations. These differences can be traced back to different factors such as the adaption of 2D plane-strain settings, which yields a stiffer behavior. Moreover, in the PFM and depending on the values of ϵ, a part of the elastic energy can locally be dissipated in the transition zone between the cracked and the uncracked regions. Therefore, the value of G_c must be in accordance with the values of ϵ and M in order to get a better quantitative convergence to the experimental results.

The effects of the internal length scale ϵ and the mobility parameter M on the pressure value needed to induce the crack for the same FE mesh and applied loadings are discussed in the following. Fig. 7 shows the fluid pressure and the phase-field time histories at point B(0.08, 0.63) considering three different values of ϵ and a constant mobility parameter $M = 10^{-3}$ m^2/N s. Apparently, the crack occurs earlier for a higher value of ϵ. In this, the local energy dissipation at crack edges is proportional to the ϵ value, and thus, lower values of the fluid pressure are needed to start the crack.

Considering a constant length scale $\epsilon = 0.01$ m and varying the value of the mobility parameter M, Fig. 8 shows that a lower value of the mobility parameter M leads to a slower crack evolution and delay of the crack occurrence. Thus, a higher pressure value is needed to induce the crack. As shown in Fig. 8, the mentioned effect of M becomes negligible for higher values of the mobility such as $M \geq 10^{-3}$ m^2/N s.

Alternatively to the application of increasing pressure at a constant rate ($\Delta\overline{p}$) to induce the crack as given in [22], the following test case considers the growth of the crack due to fluid injection at a constant rate (i.e. $\overline{Q} = n^F \mathbf{w}_F \cdot \mathbf{n} = n^F w_{F1}$) applied at the bottom of the wellbore, see Fig. 3. In Fig. 9, the fluid pressure time history is depicted at points A, B and C along the crack path. This shows an increase of the fluid pressure in the pre-crack phase until the crack occurs ($\Delta p \approx 16$MPa at point A). Thereafter, a large drop of the pressure during the crack propagation takes place ($\Delta p \approx -12.5$ MPa at point A). It is also remarkable that the crack starts at points B and C at lower pressure than that at point A. Such results agree with the description of hydraulic crack opening in a homogeneous solid given in, e.g. [44]. Comparing Fig. 9 with Fig. 6, it is also noticeable that the time needed for the crack to propagate due to fluid flux

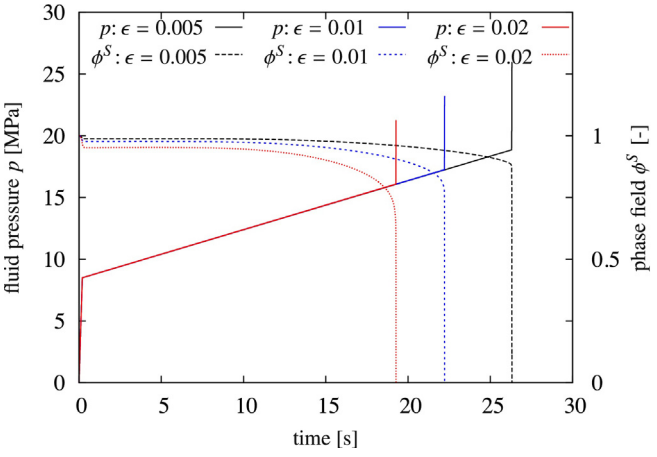

Fig. 7. Fluid pressure and phase-field time histories at point B (0.08, 0.63), which illustrate the effect of the internal length scale ϵ [m] on the pressure value needed to start the crack for the case of $\Delta\overline{p} = 0.67$ MPa/s and $M = 10^{-3}$ m^2/N s.

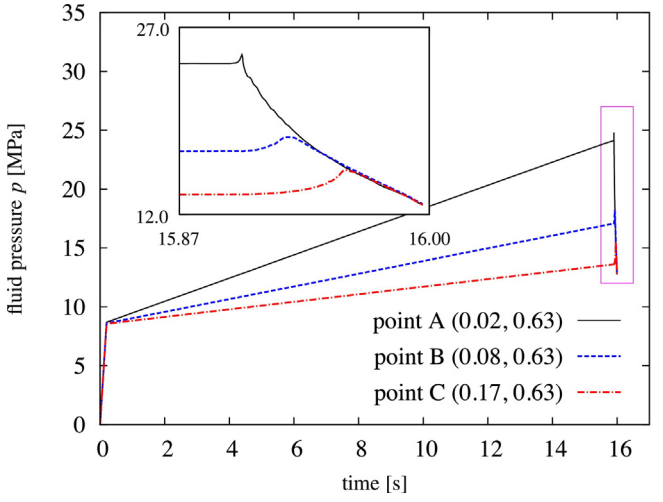

Fig. 9. Crack induced by constant fluid flux injection $\overline{Q}$ at the boundary instead of the induced increasing pressure $\Delta\overline{p}$ for the case of $M = 10^{-3}$ m^2/N s and $\epsilon = 10^{-2}$ m. A large drop of the fluid pressure is obtained after crack propagation.

injection is almost 10 times longer than that due to increasing of the pressure.

5. Conclusions

In this research work, a phase-field modeling approach to numerically simulate the hydraulic fracture of fluid-saturated heterogeneous porous materials was presented. Therefore, the continuum-mechanical Theory of Porous Media (TPM) has been employed for the mathematical modeling of the materially incompressible, biphasic medium. Furthermore, the presentation was restricted to the isothermal, small strain regime as well as quasi-static loading conditions. In order to simulate the crack evolution of the solid matrix, the TPM has been extended by a diffusive crack interface approach, allowing for a robust implementation in usual finite element codes. This extension has succeeded using a phase-field variable to distinguish between the broken and the undamaged states of the medium, whereas the well-known Allen–Cahn diffusion model was applied to calculate the evolution of the phase-field variable. This variable was also considered in the formulations of the volume fractions and the fluid permeability, which allowed to account for their permanent changes in the cracked region also after unloading. The introduced balance equations also gave the possibility to distinguish between Darcy's flow of the interstitial fluid in the porous medium and Stokes-like flow in the developed crack.

As shown in the numerical problem, the proposed approach results in a good qualitative agreement with other hydraulic fracture models and experiments introduced in the literature. To mention two aspects as an example, the crack propagates perpendicular to the maximum principal stress, and the fluid pressure suddenly increases upon occurrence of the crack and then drops and fluctuates in coincidence with crack propagation. In this regard, it is remarkable that the fluid pressure behavior in the post-crack phase differs if the crack is induced by increasing the fluid flux or the fluid pressure at the boundary, where the large drop of the fluid pressure coincides with the application of fluid flux at the boundary.

To this end, the presented research work can serve as a base for future studies and real applications in the field of porous media fracture. However, this work remains to have improvement areas. The outlook of this will be to test and compare different phase-field evolution approaches to better simulate and control the crack propagation speed and the pore-pressure behavior in the post-crack phase. Moreover, it is our intention to implement a ductile phase-field hydraulic fracture model, as well as to extend the modeling to 3D settings in order to get quantitatively better results.

Appendix A. Analytical integration of the solid volume balance equation

For the integration of the solid volume balance equation $(n^S)'_S = -n^S \operatorname{div}\mathbf{v}_S$ over time $[t_0,t]$, and considering n^S_ϕ as the initial solid volume fraction and n^S as the actual one, we start with the material time derivative of the determinant of the material deformation gradient $\det\mathbf{F}_S$

$$\begin{aligned}(\det\mathbf{F}_S)'_S &= \frac{\partial(\det\mathbf{F}_S)}{\partial\mathbf{F}_S}\cdot\frac{\mathrm{d}\mathbf{F}_S}{\mathrm{d}t},\\ &= \det\mathbf{F}_S\,\mathbf{F}_S^{T-1}\cdot\mathbf{L}_S\mathbf{F}_S,\\ &= \det\mathbf{F}_S\operatorname{div}\mathbf{v}_S,\end{aligned} \tag{A.1}$$

with $\mathbf{L}_S := \operatorname{div}\mathbf{v}_S$ being the spatial velocity gradient. Following this, the solid volume balance reads

$$\begin{aligned}&\frac{(n^S)'_S}{n^S} = -\frac{(\det\mathbf{F}_S)'_S}{\det\mathbf{F}_S},\\ &[\ln(n^S)]'_S = -[\ln(\det\mathbf{F}_S)]'_S,\\ &\int_{t_0}^{t}[\ln(n^S)]'_S\mathrm{d}t = -\int_{t_0}^{t}[\ln(\det\mathbf{F}_S)]'_S\mathrm{d}t,\\ &\ln(n^S)-\ln(n^S_\phi) = -[\ln(\det\mathbf{F}_S)-\ln(\det\mathbf{F}_{S0})],\\ &\ln\frac{n^S}{n^S_\phi} = \ln\frac{1}{\det\mathbf{F}_S},\end{aligned} \tag{A.2}$$

with $\mathbf{F}_{S0}=\mathbf{I}$ for an undeformed initial state. Following this, the explicit relation of n^S becomes

$$n^S = n^S_\phi\det\mathbf{F}_S^{-1}. \tag{A.3}$$

References

[1] M. Ambati, T. Gerasimov, L.D. Lorenzis, A review on phase-field models of brittle fracture and a new fast hybrid formulation, Comput. Mech. 55 (2015) 383–405.
[2] H. Amor, J.-J. Marigo, C. Maurini, Regularized formulation of the variational brittle fracture with unilateral contact: numerical experiments, J. Mech. Phys. Solids 57 (8) (2009) 1209–1229.
[3] A.W. Bishop, The effective stress principle, Teknisk Ukeblad 39 (1959) 859–863.
[4] M.J. Borden, C.V. Verhoosel, M.A. Scott, T.J.R. Hughes, C.M. Landis, A phase-field description of dynamic brittle fracture, Comput. Methods Appl. Mech. Eng. 217–220 (2012) 77–95.
[5] B. Bourdin, G. Francfort, J. Marigo, The variational approach to fracture, J. Elast. 91 (2008) 5–148.
[6] B. Bourdin, G. Francfort, J.-J. Marigo, Numerical experiments in revisited brittle fracture, J. Mech. Phys. Solids 48 (2000) 797–826.
[7] R.M. Bowen, Theory of mixtures, in: A.C. Eringen (Ed.), in: Continuum Physics, vol. III, Academic Press, New York, 1976, pp. 1–127.
[8] J.W. Cahn, J.E. Hilliard, Free energy of a nonuniform system. I. Interfacial free energy, J. Chem. Phys. 28 (1958) 258–267.
[9] R. de Boer, Theory of Porous Media, Springer-Verlag, Berlin, 2000.
[10] R. de Boer, W. Ehlers, The development of the concept of effective stresses, Acta Mech. 83 (1990) 77–92.
[11] W. Ehlers, Foundations of multiphasic and porous materials, in: W. Ehlers, J. Bluhm (Eds.), Porous Media: Theory, Experiments and Numerical Applications, Springer-Verlag, Berlin, 2002, pp. 3–86.
[12] C.A. Felippa, K.C. Park, C. Farhat, Partitioned analysis of coupled mechanical systems, Comput. Methods Appl. Mech. Eng. 190 (2001) 3247–3270.
[13] G. Francfort, J.-J. Marigo, Revisiting brittle fracture as an energy minimization problem, J. Mech. Phys. Solids 46 (1998) 1319–1342.
[14] A.A. Griffith, The phenomena of rupture and flow in solids, Philos. Trans. R. Soc. Lond. A 221 (1921) 163–198.
[15] P. Haupt, Foundation of continuum mechanics, in: K. Hutter (Ed.), Continuum Mechanics in Environmental Sciences and Geophysics, CISM Courses and Lectures, vol. 337, Springer-Verlag, Wien, 1993, pp. 1–77.
[16] Y. Heider, Saturated Porous Media Dynamics with Application to Earthquake Engineering. Dissertation, Report No. II-25 of the Institute of Applied Mechanics (CE), University of Stuttgart, Germany, 2012.
[17] G.R. Irwin, Analysis of stresses and strains near the end of a crack traversing a plate, J. Appl. Mech. 24 (1957) 361–364.
[18] F. Kraaijeveld, J.M. Huyghe, Propagating cracks in saturated ionized porous media, in: R. de Borst, E. Ramm (Eds.), Multiscale Methods in Computational Mechanics, Lecture Notes in Applied and Computational Mechanics, vol. 55, Springer, Dordrecht, 2011.
[19] C. Kuhn, R. Müller, A continuum phase field model for fracture, Eng. Fract. Mech. 77 (2010) 3625–3634.
[20] C. Kuhn, A. Schlüter, R. Müller, A phase field approach for dynamic fracture, PAMM 13 (1) (2013) 87–88, http://dx.doi.org/10.1002/pamm.201310039.
[21] S. Lee, A. Mikeli, M.F. Wheeler, T. Wick, Phase-field modeling of proppant-filled fractures in a poroelastic medium, Comput. Methods Appl. Mech. Eng. (2016), http://dx.doi.org/10.1016/j.cma.2016.02.008.
[22] L. Li, C. Tang, G. Li, S. Wang, Z. Liang, Y. Zhang, Numerical simulation of 3D hydraulic fracturing based on an improved flow-stress-damage model and a parallel fem technique, Rock Mech. Rock Eng. 45 (2012) 801–818.
[23] B. Markert, A constitutive approach to 3-D nonlinear fluid flow through finite deformable porous continua, Transp. Porous Med. 70 (2007) 427–450.
[24] B. Markert, Weak or Strong – On Coupled Problems in Continuum Mechanics, Habilitation, Report No. II-20 of the Institute of Applied Mechanics (CE), University of Stuttgart, 2010.
[25] B. Markert, A survey of selected coupled multifield problems in computational mechanics, J. Coupled Syst. Multiscale Dyn. 27 (2013) 22–48.

[26] B. Markert, Y. Heider, Coupled multi-field continuum methods for porous media fracture, in: M. Mehl, M. Bischoff, M. Schäfer (Eds.), Recent Trends in Computational Engineering – CE2014, Lecture Notes in Computational Science and Engineering, vol. 105, Springer International Publishing, 2015, pp. 167–180.
[27] B. Markert, Y. Heider, W. Ehlers, Comparison of monolithic and splitting solution schemes for dynamic porous media problem, Int. J. Numer. Methods Eng. 82 (2010) 1341–1383.
[28] H.G. Matthies, R. Niekamp, J. Steindorf, Algorithms for strong coupling procedures, Comput. Methods Appl. Mech. Eng. 195 (2006) 2028–2049.
[29] C. Miehe, M. Hofacker, F. Welschinger, A phase field model for rate-independent crack propagation: robust algorithmic implementation based on operator splits, Comput. Methods Appl. Mech. Eng. 199 (2010) 2765–2778.
[30] C. Miehe, S. Mauthe, S. Teichtmeister, Minimization principles for the coupled problem of darcybiot-type fluid transport in porous media linked to phase field modeling of fracture, J. Mech. Phys. Solids 82 (2015) 186–217.
[31] A. Mikelić, M.F. Wheeler, T. Wick, A phase-field method for propagating fluid-filled fractures coupled to a surrounding porous medium, Multiscale Model Simul. 13 (1) (2015) 367–398.
[32] A. Mikelić, M.F. Wheeler, T. Wick, A quasi-static phase-field approach to pressurized fractures, Nonlinearity 28 (5) (2015) 1371–1399.
[33] N. Moelans, B. Blanpain, P. Wollants, An introduction to phase-field modeling of microstructure evolution, Calphad 32 (2) (2008) 268–294.
[34] D. Mumford, J. Shah, Optimal approximation of piecewise smooth functions and associated variational problems, Commun. Pure Appl. Math. 42 (1989) 577–685.
[35] C.H. Padilla, B. Markert, A coupled ductile fracture phase-field model for crystal plasticity, Contin. Mech. Therm. (2015) 1–10.
[36] S.P. Patil, Y. Heider, C. Hernandez-Padilla, E. Cruz-Chú, B. Markert, A comparative molecular dynamics-phase-field modeling approach to brittle fracture, Comput. Methods Appl. Mech. Eng. (2016), doi:10.1016/j.cma.2016.04.005.
[37] G. Pijaudier-Cabot, G. Dufour, M. Choinska, Permeability due to the increase of damage in concrete: from diffuse to localized damage distributions, J. Eng. Mech. ASCE 135 (2009) 1022–1028.
[38] A. Prohl, Projection and Quasi-Compressibility Methods for Solving the Incompressible Navier–Stokes Equations, Teubner, Stuttgart, 1997.
[39] J. Réthoré, R. de Borst, M. Abellan, A two-scale approach for fluid flow in fractured porous media, Int. J. Numer. Methods Eng. 71 (7) (2007) 780–800.
[40] J. Réthoré, R. de Borst, M. Abellan, A two-scale model for fluid flow in an unsaturated porous medium with cohesive cracks, Comput. Mech. 42 (2) (2008) 227–238.
[41] A. Schlüter, A. Willenbücher, C. Kuhn, R. Müller, Phase field approximation of dynamic brittle fracture, Comput. Mech. 54 (2014) 1141–1161.
[42] S. Secchi, B. Schrefler, A method for 3-D hydraulic fracturing simulation, Int. J. Fract. 178 (1–2) (2012) 245–258.
[43] S. Secchi, L. Simoni, B.A. Schrefler, Hydraulic fracturing and its peculiarities, Asia Pac. J. Comput. Eng. (2014), doi:10.1186/2196-1166-1-8.
[44] F. Tzschichholz, H.J. Herrmann, Simulations of pressure fluctuations and acoustic emission in hydraulic fracturing, Phys. Rev. E 51 (1995 Mar) 1961–1970.
[45] K. Weinberg, C. Hesch, A high-order finite deformation phase-field approach to fracture, Contin. Mech. Thermodyn. (2015), http://dx.doi.org/10.1007/s00161-015-0440-7.
[46] O.C. Zienkiewicz, R.L. Taylor, The Finite Element Method. The Basis, vol. 1, 5th edition, Butterworth Heinemann, Oxford, 2000.